J Solid State Electrochem (2012) 16:2709–2715
DOI 10.1007/s10008-012-1685-8

ORIGINAL PAPER

Modification of growth parameters of Ti anodic films by fluoride ion insertion

Próspero Acevedo-Peña · Ignacio González

Received: 26 October 2011 / Revised: 7 February 2012 / Accepted: 9 February 2012 / Published online: 1 March 2012

Abstract The potentiostatic growth of Ti anodic films formed in 0.1 M $HClO_4$/xM HF (0.05 M≤x≤0.50 M) media was studied by electrochemical impedance spectroscopy, EIS. The obtained EIS spectra were analyzed by using the surface charge approach model, which showed oxide growth parameters being modified as the HF concentration increased. While the electric field through the film decreased, oxide growth rate and atomic half jump distance increased, evidencing that fluoride ions are inserted into the oxide through oxygen vacancies, thereby modifying the lattice structure and electric properties of the oxide. Additionally, the experimental data obtained for the pseudocapacitance C_0, appearing at low-frequency domain, allowed the interpretation commonly given for this element (modulation of film thickness) to be discarded; instead, the F^- ion diffusion coefficient was estimated, casting with variation of electric properties with HF concentration and E_F.

Keywords Anodic films · Fluoride ion insertion · Surface charge approach model · EIS

Introduction

Fundamental studies dedicated to the comprehension of self-organized porous structures show that the insertion of fluoride ions occurring during the anodized process plays a very important role in the formation of these structures; however, this is still not clearly established [1]. There are evidences for the formation, at the Ti/oxide interface, of a film rich in fluoride ions, which are inserted into oxygen vacancies and rapidly spread due to the electric field imposed to form the film [2]. In addition, the great ion mobility, partially caused by insertion of F^- ions, seems to be responsible for the increase in the coefficient of volumetric expansion, usually reported for this type of structures [3]. Then, the F^- ions that are inserted into the oxide must modify anodic film properties to some extent and be involved in the mechanism for the formation of self-organized porous structures; however, this is not clearly established in the literature.

The surface charge approach model has been shown to be efficient in the study and description of the growth of oxide films under oxidation/dissolution conditions [4, 5], allowing the estimation of different parameters involved in film growth. The evaluation of these parameters would allow the clarification of the effect of fluoride ion insertion on the properties of the compact oxide film formed at the Ti/oxide interface. For this reason, the estimation of parameters of the oxide film growth during Ti anodization in 0.1 M $HClO_4$/xM HF (0.05 M≤x≤0.50 M) solutions was carried out in our study using the surface charge approach model.

Experimental

The electrodes employed herein were made from a 99.99% purity Alfa Aesar Ti rod, embedded with Teflon, and with a 0.283-cm^2 circular area left uncovered. They were polished with a series of silicon carbide emery papers, subsequently obtaining a mirror-like finish with 50-nm aluminum in an automatic Buehler Minimet 1000 polisher. This was to ensure the same initial conditions for all electrochemical studies.

The electrochemical tests were performed in a conventional three-electrode cell. A platinum wire was used as the

P. Acevedo-Peña · I. González (✉)
Laboratory of Electrochemistry, Department of Chemistry,
Universidad Autónoma Metropolitana-Iztapalapa (UAM-I),
Apdo. Postal 55-534,
09340 Ciudad de México, DF, Mexico
e-mail: igm@xanum.uam.mx

pseudoreference electrode. The counter electrode was a graphite rod (99.999% Alfa Aesar). The electrolytes were prepared using milli-Q water (18.2 MΩ/cm), HF (99.99% Alfa Aesar), and $HClO_4$ (69.72% Alfa Aesar). Prior to each test, the solution was bubbled with N_2 for 15 min.

The film growth and electrochemical impedance spectroscopy (EIS) measurements were carried out with an EG&G PAR model 283 potentiostat/galvanostat, coupled to a SI model 1260 Solartron frequency response analyzer.

Results and discussion

Potentiostatic anodization

Voltammetric curves obtained in electrolytes with different HF concentrations (not shown), exhibited a wide potential window for passive film formation, as has been previously reported by other researchers [6]. In this study, potentiostatic anodization was carried out at five different formation potentials, E_F (0.5, 2.5, 4.5, 6.5, and 8.0 V). Steady-state currents, i_{ss}, obtained after 2.5 h of anodization, were slightly affected by the imposed E_F, as compared to the influence of HF concentration; for this reason, the average i_{ss} of the films formed at different E_F, for each of the HF concentrations evaluated (0.05, 0.10, 0.25, and 0.50 M), is plotted in Fig. 1.

Linear dependence of i_{ss} on HF concentration, in a double-logarithmic chart, has also been reported for Nb [7], with a slope (1.22) similar to that found in this study. This was attributed to oxide dissolution, caused by the attack of F^- ions that, for the particular case of Ti, is described in the following equation [1, 2]:

$$TiO_2 + 4H_3O^+ + 6F^- \rightarrow (TiF_6)^{2-} + 6H_2O \quad (1)$$

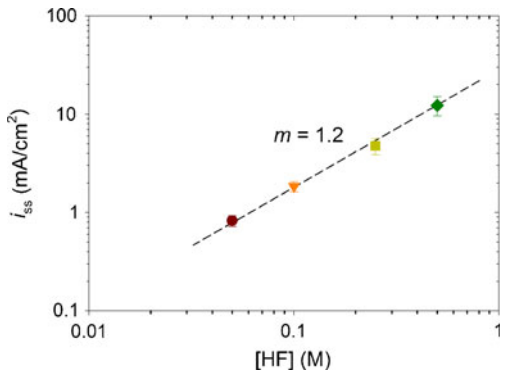

Fig. 1 Variation of the steady-state current (i_{ss}) obtained after 2.5 h of potentiostatic anodization of Ti, with HF concentration present in a 0.1-M $HClO_4$/xM HF solution. Each point corresponds to the average i_{ss}, obtained for the films formed at different formation potentials E_F (0.5, 2.5, 4.5, 6.5, and 8.0 V). The slope (m) of this curve is indicated in the figure

EIS characterization

Figure 2 shows impedance plots obtained experimentally (steady state) after 2.5 h of anodization, evidencing the effect of HF concentration (Fig. 2a, b, and c) and the effect of E_F imposed to form the film (Fig. 2d, e, and f).

Impedance plots show the presence of three time constants [5–12]: in the high-frequency region, a behavior observed is typical of the resistor–capacitor (RC) circuit, due to the resistance and capacitance of the oxide film formed at the metal surface. Subsequently, inductance is observed; this is commonly related to the adsorption of negatively charged species, in this case, F^- ions, at the oxide surface [9]. Eventually, at lower frequencies, a capacitive behavior appears; the physical meaning of this component keeps being a little controversial, the reason for which will be discussed further on [8–10, 12].

The variation in HF concentration caused significant variations in impedance plots (Fig. 2a, b, and c). In general, the increase in concentration leads to a decrease in the magnitude of impedances in the high-frequency region (Fig. 2a and c), accompanied by a decrease in the phase angle (Fig. 2b). The inductive loop was also affected and appeared at higher frequencies (Fig. 2b and c), and with a smaller impedance (Fig. 2a and c), at increased HF concentration. In the Nyquist plot (Fig. 2a), the capacitive element at low frequencies seems not to be affected by the increase in HF concentration; however, at Bode plot of phase angle, it is clearly seen how it acquires increasingly higher values with the increment in concentration (Fig. 2b).

The increase in E_F imposed to form the films also resulted in changes in impedance spectra obtained (Fig. 2d, e, and f) mainly appearing in the variation in RC components present at high frequencies, and inductance, present at intermediate frequencies. In addition, the increase in E_F made the capacitive element normally present at low frequencies appear at increasingly lower frequencies; however, this variation is not as important as that observed with the rise in HF concentration.

Electric equivalent circuit

The obtained impedance spectra were fitted adequately ($\chi^2 < 10^{-4}$) to the surface charge approach model proposed by Bojinov, which can be represented by electric equivalent circuit, *eec*, shown in Fig. 3 [4, 5]. This *eec* has solution resistance, R_S, in series with a pseudocapacitor C_0, associated with oxide layer thickness modulation at low frequencies. These elements are connected in series to a circuit consisting of the capacitance C_b, representing the capacitance of the compact oxide layer on the electrode, in parallel with the

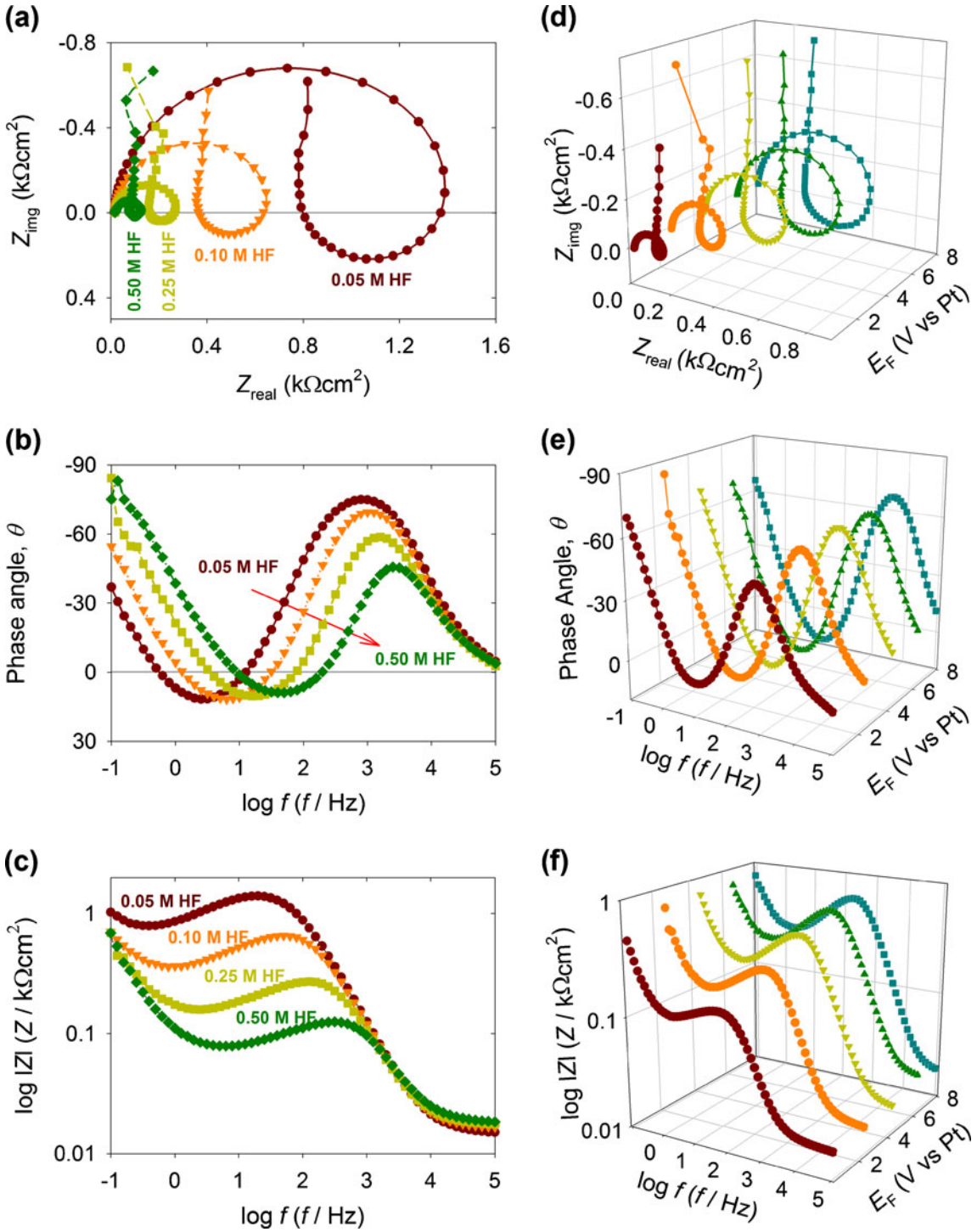

Fig. 2 Impedance spectra obtained experimentally after 2.5 h of Ti anodization in 0.1 M $HClO_4$/xM HF solutions. Nyquist (**a** and **d**) and Bode plots of phase angle (**b** and **e**) and impedance magnitude (**c** and **f**). Plots in **a**, **b**, and **c** show the effect of HF concentration after imposing an E_F of 2.5 V. Plots in **d**, **e**, and **f** show the effect of formation potential, E_F, in the 0.1-M $HClO_4$/0.25-M HF solution

oxide film resistance, R_b, the resistance R_{SC}, and inductance L_{SC}, related to the generation of a negative surface excess charge that causes an increase in oxygen vacancy transport.

As observed in Fig. 3, this *eec* allows an adequate fit to experimental data ($\chi \approx 10^{-4}$). The region of high frequencies is controlled by the resistance and capacitance of the oxide film, R_b and C_b (continuous line). At intermediate frequencies, an inductive loop appears due to R_{SC} and L_{SC} (dotted line). At low frequencies, the phase angle variation is due to the pseudocapacitance C_0 (dashed line).

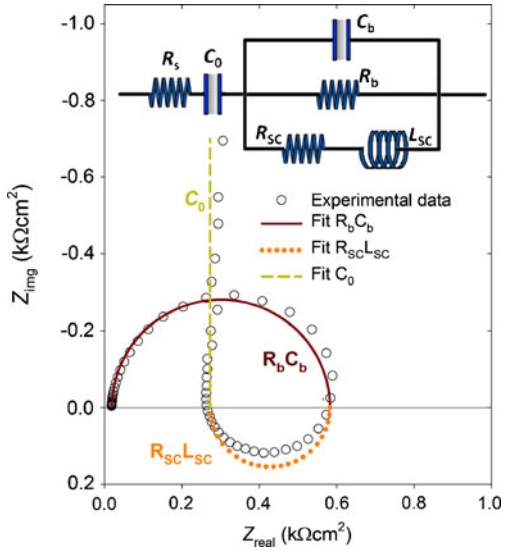

Fig. 3 Electric equivalent circuit according to the surface charge approach model [4, 5], employed for the fitting of the experimentally obtained impedance spectra. The fitting to an experimental spectrum for a film growth at 0.25 M HF and E_F of 8.0 V is shown as an example. The experimental data are represented by the *empty circles*. The region of high frequencies is controlled by the resistance and capacitance of the oxide film, R_b and C_b (*continuous line*). At intermediate frequencies, an inductive loop appears due to R_{SC} and L_{SC} (*dotted line*). At low frequencies, the phase angle variation is due to the pseudocapacitance C_0 (*dashed line*)

The surface charge approach model predicts the following expressions for the components of *eec* in Fig. 3 [4, 5, 7, 8]:

$$\frac{d(R_b i_{ss})}{dE_F} = \frac{RT}{zFaV_F} \tag{2}$$

$$\frac{d(d_{ox})}{dE_F} = \frac{(1-\alpha)}{V_F} \tag{3}$$

$$\frac{L_{SC} i_{ss}}{R_{SC}} = S^{-1} \tag{4}$$

$$\frac{R_b}{R_{SC}} = \frac{\alpha}{(1-\alpha)} \tag{5}$$

$$C_0 = \frac{nF(1-\alpha)}{V_m \lambda V_F} \tag{6}$$

where z is the electric charge of mobile species (oxygen vacancies), a is the atomic half jump distance, V_F is the electric field in oxide film, d_{ox} is the thickness of the oxide film formed, α is the polarizability of the oxide/solution interface, n is the number of elementary charges necessary to form an oxide molecule, V_m is the molar volume of the formed oxide, λ is the current efficiency in oxide formation, and S is the cross-capture section.

Values of the *eec* elements of Fig. 3, derived from the best fit to experimentally obtained impedance spectra, Fig. 2, are summarized in Table 1. The relationships proposed by surface charge approach model [2–4, 6], using the estimated values from *eec*, show a linear dependence with E_F (Fig. 4b, c, and d), as this model predicts.

The thickness of the oxide film formed, d_{ox}, was estimated from the value of C_b, using Eq. 7 [7, 9]:

$$\left(\frac{1}{C_b} - \frac{1}{C_H}\right)^{-1} = \frac{\varepsilon \times \varepsilon_0}{d_{ox}} \tag{7}$$

where C_H is the electric double-layer capacitance (assumed as 20 μF/cm^2 [13]), ε_0 is the vacuum permittivity (8.85× 10^{-14} F/cm), and ε is the dielectric constant of the oxide film (assumed as 50 [14]).

The dependence of d_{ox} on E_F is linear (Fig. 4a) as predicted by the oxide film growth model [4–9]; however, it is worth mentioning that, although this dependence remained with higher HF concentration in the solution, the slope of this straight line became increasingly greater, showing an increment in film growth ratio with a higher HF concentration in the solution (Fig. 4a).

Parameters S and α were estimated from Eqs. 4 and 5 that predict a linear dependence between R_{SC} vs $L_{SC} \times i_{ss}$ (Fig. 5a) and R_b vs R_{SC} (Fig. 5b), respectively. These ratios proved to be really independent of E_F during anodization, varying only with HF concentration in the case of α (Fig. 5b), but remaining even independent of the concentration in the case of S (Fig. 5a). Values of V_F, a, d_{ox} and λ; parameters were estimated from Eqs. 2, 3, and 6. All values obtained are summarized in Table 2.

Unfortunately, there are no researches in the literature reporting values of these parameters for anodic Ti films, formed potentiostatically in media containing fluorides. Nevertheless, different tendencies observed in the values of these parameters for growing anodic films on other metallic materials (Nb [6] and W [15]) in media containing fluoride ions, and those obtained herein, indicate that modifications generated by F^- ions may depend on the nature of oxide formed on the metallic surface.

The independence of S, cross-capture section, both from E_F and HF concentration, indicates that despite the inductive component appearing at increasingly higher frequencies, which shows that oxygen vacancy transport becomes increasingly faster due to the formation of an excess negative charge at the oxide/solution interface, the amount of F^- ions adsorbed at the oxide surface is not being modified by HF concentration. For their part, both α (oxide/solution interface polarizability) and V_F (electric field through the oxide film) acquired smaller values with higher HF concentration indicating that the potential through the oxide is increasingly lower; this justifies the increase in the anodic film growth

Table 1 Values of electric components (from *eec* in Fig. 3) obtained from the best fit of EIS spectra of TiO_2 anodic films formed at different E_F in 0.1 M $HClO_4$/*x*M HF media (*x* values are indicated in the table)

[HF]	E_F(V)	C_0(mF/cm^2)	R_b(kΩcm^2)	C_b(μF/cm^2)	R_{SC}(kΩcm^2)	L_{SC}(F/cm^2)
0.05 M	0.5	12.48	0.74	13.42	1.84	198.14
	2.5	8.97	1.39	4.61	1.86	153.94
	4.5	8.26	2.22	2.85	2.26	176.06
	6.5	8.03	3.31	2.02	2.99	247.68
	8	8.11	3.21	1.69	3.12	263.40
0.1 M	0.5	11.68	0.40	11.49	0.88	32.49
	2.5	9.41	0.64	4.70	0.79	23.01
	4.5	7.93	0.93	2.68	0.93	25.32
	6.5	7.43	1.50	1.72	1.27	40.31
	8	7.39	1.70	1.47	1.39	46.71
0.25 M	0.5	12.56	0.14	15.13	0.43	6.69
	2.5	9.21	0.25	5.09	0.34	3.48
	4.5	7.99	0.39	2.65	0.40	4.55
	6.5	7.57	0.50	1.75	0.44	4.77
	8	7.42	0.56	1.38	0.46	4.46
0.5 M	0.5	12.34	0.05	17.28	0.20	1.15
	2.5	8.65	0.10	4.57	0.15	0.58
	4.5	8.97	0.17	2.27	0.16	0.65
	6.5	7.95	0.21	1.46	0.18	0.62
	8	8.22	0.24	1.27	0.20	0.68

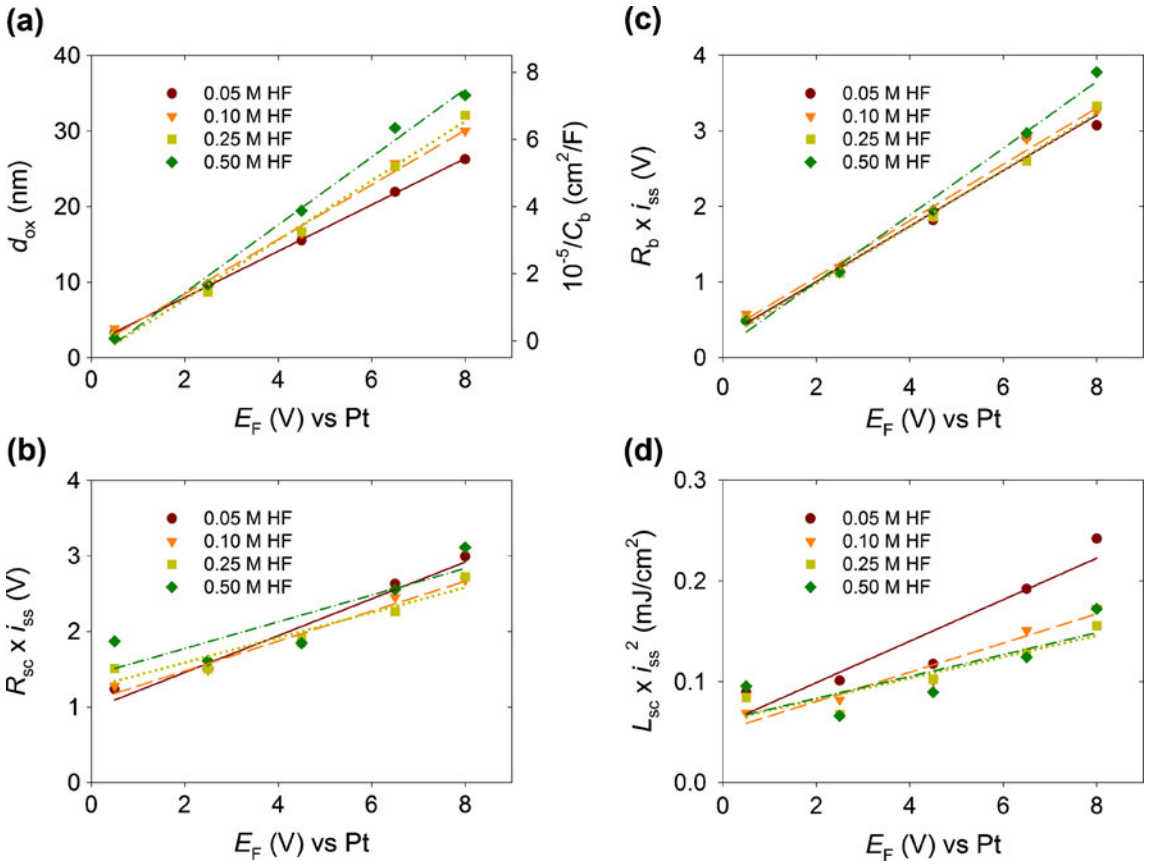

Fig. 4 Influence of formation potentials (E_F) of anodic films on the electric equivalent circuit elements (Fig. 3) measured when the steady-state current (i_{ss}) was reached: **a** C_b, **b** R_{SC}, **c** R_b, and **d** L_{SC}

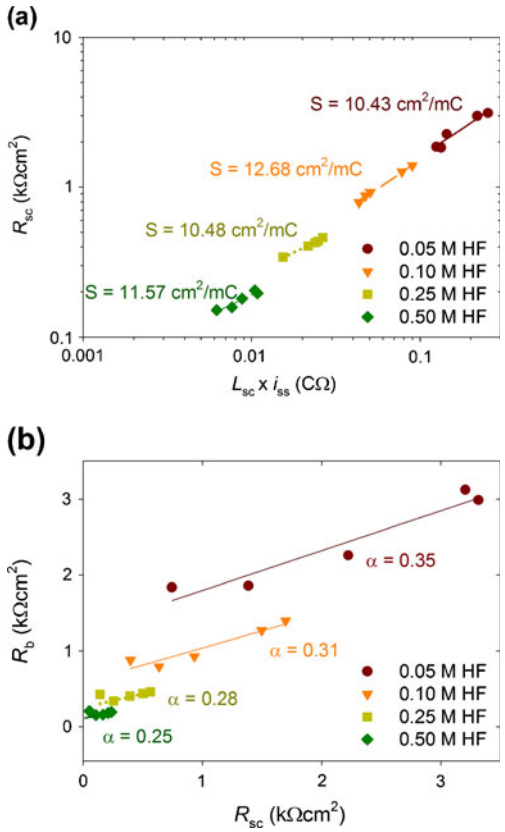

Fig. 5 Graphical estimation of the **a** cross-capture section S (square centimeters per millicoulumb (cm^2/mC)) and **b** polarizability of the oxide/solution interface α from relations in Eqs. 4 and 5

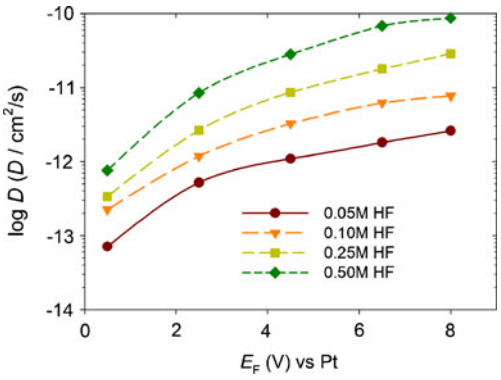

Fig. 6 Influence of the formation potential, E_F, over the fluoride ion diffusion coefficient, D (square centimeters per second), for the film's growth in solutions 0.1 M $HClO_4$/xM HF. x values are indicated in the figure

rate d(d_{ox})/dE_F. Furthermore, the atomic half jump distance (a) acquired increasingly greater values with higher HF concentration indicating that the lattice structure gets deformed by the insertion of fluoride ions.

In addition, the current efficiency in oxide formation (λ) had values closer to 1 at higher HF concentration, contradicting the expectation due to greater chemical attack of the oxide formed in these solutions [1, 6, 10, 12]. A value of 1 for λ has also been reported by Jović et al. [8] for the growth of Nb anodic films in concentrated NaOH media, which casts doubt upon the physical meaning proposed by the surface charge approach model [4, 5] for this element.

Normally, the value of estimated oxide growth rate of C_0, using Eq. 6 and assuming that λ is 1, overestimates the oxide film growth ratio. However, in the present case, although d(d_{ox})/dE_F increased with HF concentration, the value of C_0 did not and exhibited values that can be considered to be independent of the conditions of film formation (E_F and [HF]) [8]; see Table 1. This opens up discussion on the adequate physical meaning of this element. It is important to point out that even at the lowest E_F considered (0.5 V), the C_0 is independent of concentration, and its value is different from that obtained at higher E_F.

Kong has recently proposed [9], similarly to the case of insertion of Li^+ and H^+, that the pseudocapacitance (C_0) can be associated to insertion and diffusion of F^- ions, estimating a diffusion coefficient of F^-, six orders of magnitude higher than the diffusion coefficient of oxygen vacancies. Replacing the capacitance C_0 in *eec* (Fig. 3) by a diffusion element, whose impedance is described by the finite-length diffusion model [9], the diffusion coefficient of F^- ions within oxide film, D, may be estimated from the product between the square of the compact layer thickness (d_{ox}, Fig. 4a) and the characteristic frequency of this diffusion element (ω_0) that corresponds to the frequency at which pseudocapacitive behavior starts to be detected, Eq. 8.

$$D = d_{ox}^2 \times \omega_0 \tag{8}$$

The values of D, estimated for the films formed in the different electrolytes, as a function of the formation potential, E_F, to each HF concentration employed in this study, are shown in Fig. 6. The D dependence with E_F is the same reported by Kong [9]. The increase of HF concentration does not change the shape of the curves, but it provoked an increase in the D

Table 2 Kinetic parameters of the potentiostatic growth of passive Ti films in 0.1 M $HClO_4$/x M HF media, obtained from EIS analysis in the frame of surface charge approach model

[HF] (M)	α	S (cm^2/mC)	V_F (MV/nm)	a (Å)	d(d_{ox})/dE_F (nm/V)	λ
0.05	0.35	10.43	2.13	2.16	3.07	0.70
0.10	0.31	12.68	1.91	2.45	3.61	0.86
0.25	0.28	10.48	1.84	2.55	3.93	0.92
0.50	0.25	11.57	1.66	3.34	4.49	1.00

values estimated. The increase in the value of D with the HF concentration supports the changes observed in growth parameters justifying the oxide growth ration increase, the electric field decrease through it due to the change in electric properties, and the increase in atomic half jump distance, because of oxide lattice structure deformation.

Conclusions

The analysis of the EIS spectra obtained during Ti anodic film growth in 0.1 M $HClO_4$/xM HF (0.05 M≤x≤0.50 M) solutions, by the surface charge approach model, showed that oxide growth parameters were modified as the HF concentration increased. These modifications seem to be carried by the insertion of the fluoride ions into the oxide through oxygen vacancies, thereby modifying the lattice structure and electric properties of the oxide. Additionally, the experimental data obtained for the pseudocapacitance C_0, appearing at low-frequency domain, allowed the interpretation commonly given for this element (modulation of film thickness) to be discarded; instead, the F^- ion diffusion coefficient was estimated, casting with the variation of electric properties with HF concentration and E_F.

Different studies are being performed in our laboratory to establish a possible relationship between the modification of properties in the passive film formed and the final morphology obtained, specifically the formation of self-organized nanopore or nanotube films.

Acknowledgments This work has been given the financial support from CONACyT (Project CB-2008/105655). Próspero Acevedo Peña is grateful to CONACyT for the PhD grant through the program *doctorados nacionales*.

References

1. Roy P, Berger S, Schmuki P (2011) Agnew Chem Int Ed 50:2904–2939
2. Albu SP, Ghicov A, Aldabergenova S, Drechsel P, LeClere D, Thompson GE, Macak JM, Schmuki P (2008) Adv Mater 20:4125–4139
3. Hebert KR, Houser JE (2009) J Electrochem Soc 156:C275–C281
4. Bojinov M (1997) J Solid State Electrochem 1:161–171
5. Bojinov M (1997) Electrochim Acta 42:3489–3498
6. Frateur I, Cattarin S, Musiani M, Tribollet B (2002) J Electroanal Chem 482:202–210
7. Cattarin S, Musiani M, Tribollet B (2002) J Electrochem Soc 149: B457–B464
8. Jović VD, Jović BM (2008) J Serb Chem Soc 73:351–367
9. Kong D-S (2010) Langmuir 26:4880–4891
10. Acevedo-Peña P, González I (2011) ECS Trans 36:257–265
11. Peñafiel-Castro JA, Quintero-Torres R, de Taconi NR, Rajeshwar K, Chanmanee W (2011) J Electrochem Soc 158:D84–D90
12. Acevedo-Peña P, González I (2012) J Electrochem Soc 159:C101–C108
13. Di Quarto F, Di Paola A (1980) Sunser. J Electrochem Soc 127:1016–1021
14. Acevedo-Peña P, Vázquez G, Laverde D, Pedraza-Rosas JE, Manríquez J, González I (2009) J Electrochem Soc 156: C377–C386
15. Karastoyanov V, Bojinov M (2008) Mater Chem Phys 112:702–710